Journal of the European Ceramic Society 23 (2003) 873–881

www.elsevier.com/locate/jeurceramsoc

Phase transformation, reaction kinetics and microwave characteristics of Bi_2O_3–ZnO–Nb_2O_5 ceramics

San-Yuan Chen[a,*], Shinn-Yih Lee[b], Yih-Jaw Lin[a]

[a]*Department of Materials Science and Engineering, National Chiao-Tung University, Hsinchu, 300, Taiwan, ROC*
[b]*Department of Ceramic and Material Science, National Lien-Ho Institute of Technology, 1 Lien-Kung, Kung-Ching Li, Miao Li, Taiwan, ROC*

Received 28 December 2001; received in revised form 4 June 2002; accepted 16 June 2002

Abstract

Oxide powders of Bi_2O_3, ZnO and Nb_2O_5 were used to investigate the phase transformation, reaction kinetics and microwave properties of both $Bi_2(Zn_{1/3}Nb_{2/3})_2O_7$ and $(Bi_{1.5}Zn_{0.5})(Zn_{0.5}Nb_{1.5})O_7$ phases in the Bi_2O_3–ZnO–Nb_2O_5 system. Kinetic studies indicate that the formation mechanism of $Bi_2(Zn_{1/3}Nb_{2/3})_2O_7$ phase belongs to diffusion controlled reaction with a zero nucleation rate. In contrast, $(Bi_{1.5}Zn_{0.5})(Zn_{0.5}Nb_{1.5})O_7$ phase was interpreted as diffusion controlled reaction with a constant nucleation rate with either $Bi_5Nb_3O_{15}$ or $BiNbO_4$ phases as the nuclei. Furthermore, a lower activation energy and formation temperature were observed in the $(Bi_{1.5}Zn_{0.5})(Zn_{0.5}Nb_{1.5})O_7$ than $Bi_2(Zn_{1/3}Nb_{2/3})_2O_7$ phase. Additionally, the $(Bi_{1.5}Zn_{0.5})(Zn_{0.5}Nb_{1.5})O_7$ phase exhibits a higher dielectric constant but a lower Q value as compared with $Bi_2(Zn_{1/3}Nb_{2/3})_2O_7$ phase.

Keywords: Bi_2O_3–ZnO–Nb_2O_5; Microwave characteristics; Phase transformation; Reaction kinetics

1. Introduction

Mobile radio communication networks have been greatly expanded by portable and automobile telephones.[1,2] The development of multilayer devices for microwave applications has received wide attraction since these multilayer devices have unique characteristics of smaller size and high volume efficiency.[3,4] Although the techniques for the multilayer capacitors have been well developed in the past few years,[5] the requirement in either materials or internal electrodes is more important and urgent. In order to reduce the tangent loss, the electrodes with higher conductivity such as silver have to be used in the co-firing process. Therefore, it is imperative to lower the sintering temperature of microwave ceramics in order to co-fire with low loss conductors below 1000 °C.

Recently, Bi_2O_3–ZnO–Nb_2O_5 (hereafter designated as BZN) system has received wide attraction since it does present relatively low sintering temperature (less than 1000 °C) and excellent microwave properties.[6–9] Yan et al. revealed that these materials based on $Bi_2(ZnNb_2)O_9$ and $Bi_3(Ni_2Nb)O_9$ system, when sintered at the temperatures ranging from 880 to 920 °C, show large dielectric constant of 80 to 100, smaller temperature coefficients of $<20\times10^{-6}/°C$, and relatively large Q values of 2000 to 3000 in the 100 kHz to 3 MHz.[7] Swartz *et al.* disclosed that there are two distinct crystalline phases with nominal stoichiometries of $Bi_2(Zn_{1/3}Nb_{2/3})_2O_7$ and $Bi_{4/3}(Zn_{2/3}Nb_{4/3})O_6$ in BZN ceramic.[9] Both phases are pyrochlore structure which is one of the oxygen octahedron based families with the general formula written as $A_2B_2O_7$. The A cations are eight coordinated and the B cations are six-coordinated.[10,11] $Bi_2(Zn_{1/3}Nb_{2/3})_2O_7$ (termed as O–BZN) belongs to an orthorhombic pyrochlore.[12] On the other hand, according to XRD patterns $(Bi_{1.5}Zn_{0.5})(Zn_{0.5}Nb_{1.5})O_7$ (termed as C–BZN) instead of $Bi_{4/3}(Zn_{2/3}Nb_{4/3})O_6$ composition was indexed as a typical pyrochlore with a face-centered cubic cell. The relationship between $Bi_2(Zn_{1/3}Nb_{2/3})_2O_7$ and $(Bi_{1.5}Zn_{0.5})(Zn_{0.5}Nb_{1.5})O_7$ can be indicated using a common chemical formula.[12]

$$(Bi_{3x}Zn_{2-3x})(Zn_xNb_{2-x})O_7 \quad (0.5 \leqslant x \leqslant 0.66)$$

* Corresponding author: Fax: +886-3-5725490.
E-mail address: sychen@cc.nctu.edu.tw (S.-Y. Chen).

0955-2219/03/$ - see front matter
PII: S0955-2219(02)00199-1

When the x is equal to 0.5, the structure formed is close related to cubic pyrochlore. When x is equal to 0.66, the structure with orthorhombic pyrochlore phase formed. Further, a mixture of orthorhombic and cubic pyrochlores exists in the compositions with x in between 0.5 and 0.66. The related microwave properties of orthorhombic and cubic pyrochlores phases are $\varepsilon_r \sim 80$, $\tau_\varepsilon \sim +200$ ppm/°C, $\tan\delta < 0.0002$ and $\varepsilon_r \sim 145$, $\tau_\varepsilon \sim -360$ ppm/°C, $\tan\delta < 0.0002$ (100 kHz), respectively.[9] Thus, it is possible to control the temperature compensation of the dielectric permittivity by adjusting the ratio of positive-τ_ε O–BZN and negative-τ_ε C–BZN phases by modifying Bi_2O_3 content and sintering conditions. However, The undesirable Bi–Nb oxide phases such as $BiNbO_4$ and $Bi_5Nb_3O_{15}$ will be produced during calcination and makes it difficult to control the ratio of O–BZN and C–BZN phases, which further leads to inferior microwave dielectric behavior. The control in the composition and calcinations temperature plays a very important role in the phase reaction and microwave properties.[6–8] Therefore, it is imperative to understand the role of Bi-Nb oxide phases in the formation of O–BZN and C–BZN phases. Consequently, the BZN compositions corresponding to orthorhombic $Bi_2(Zn_{1/3}Nb_{2/3})_2O_7$ and cubic $(Bi_{1.5}Zn_{0.5})(Zn_{0.5}Nb_{1.5})O_7$ phases were studied in this work. The formation mechanism and reaction kinetics for both pyrochlore phases will be investigated. A possible reaction mechanism is proposed and discussed in this paper. Furthermore, the relationship between the sintering density and microwave properties of BZN ceramics is also presented.

2. Experimental procedure

2.1. Sample preparation

High-purity (more than 99.5%) Bi_2O_3 (R.D.H., Germany, 1.15 μm), ZnO (Merck 8849 Germany, 1.67 μnd Nb_2O_5 (Mitsui, Japan, 0.95 μm) powders were used to prepare xBi_2O_3–ZnO–Nb_2O_5 ($0.78 \leqslant x \leqslant 2$) multiple-oxide ceramic systems by a conventional powder-processing technique. Two major compositions—$Bi_2(Zn_{1/3}Nb_{2/3})_2O_7$ and $(Bi_{1.5}Zn_{0.5})(Zn_{0.5}Nb_{1.5})O_7$—were mainly used in this work. The weighed oxides in accordance with the compositions were mixed in deionized water with ZrO_2 as milling media in polyethylene container. A fixed amount of ~1 gm powder sample, extracted from the 100 gm batch, was subjected to calcination at 400–1000 °C for 1 min to 4 h. Each datum appearing on the calcination temperature/time curves was the average of three test results. The deviation of the data was around 5%. To reduce the influence of heating up and cooling down, calcination was conducted by directly putting the mixture sample into a furnace kept at preset temperatures. The time was measured from the instant the powder samples reached the preset temperatures, which was generally of the order of 1 min. The samples were pulled out immediately after heat treatment and air-quenched.

2.2. Characterization and microstructure analysis

X-ray diffractometer (XRD) was used to determine crystal structure. To study the formation mechanism and reaction kinetics, the relative percentage of the formed phase was calculated according to the equation,

$$P(\%) = 100 \times \frac{I_i}{\Sigma I_i (i = \text{appearing phases})} \quad (1)$$

where I_i and ΣI_i represent the individual and summary integrated intensities of the strongest diffraction peaks of the appearing phases according to ASTM JCPDS, respectively. For example, the (222) and (220) peaks were the strongest peaks in the cubic and orthorhombic pyrochlore phases, respectively. Differential thermal analysis (DTA) was also used to study the possible reactions with a heating rate of 10 °C/min. Dielectric characteristics at microwave frequencies were measured by Hakki and Coleman's dielectric resonator method,[13] as modified and improved by Courtney.[14] A cylindrically shaped dielectric resonator was positioned between two brass plates. An HP8722D network analyzer was used for the microwave measurements at 3 GHz.

3. Results and discussion

3.1. Crystal structures and phase evolution

In the Bi_2O_3–ZnO–Nb_2O_5 (BZN) system, it was reported that bismuth content exhibits a strong effect on the formation of pyrochlore phases.[12] Five compositions were used in this work as shown in Table 1 where BN1, BN2, BN3, O–BZN and C–BZN are representative of $Bi_{1.7}Nb_{0.3}O_{3.3}$, $Bi_5Nb_3O_{15}$, $BiNbO_4$, orthorhombic $Bi_2(Zn_{1/3}Nb_{2/3})_2O_7$ and cubic $(Bi_{1.5}Zn_{0.5})(Zn_{0.5}Nb_{1.5})O_7$ phases, respectively. The ratio of ZnO/Nb_2O_5 was fixed with changing Bi_2O_3 from 2 to 0.78 in the xBi_2O_3–ZnO–Nb_2O_5 compositions and labeled with A1 to A5, respectively. Typical XRD patterns of BZN ceramics sintered at 1000 °C for 1 h were shown in Fig. 1. A typical orthorhombic $Bi_2(Zn_{1/3}Nb_{2/3})_2O_7$ pyrochlore phase was observed for A2 (1.5 Bi_2O_3–ZnO–Nb_2O_5) composition. If excess Bi_2O_3 was used in the Bi_2O_3–ZnO–Nb_2O_5 system, it was found that not only O–BZN but also BN2 phases are always observed in the A1 ($2Bi_2O_3$–ZnO–Nb_2O_5) composition. The XRD patterns in Fig. 1 show that the A3 (1.25 Bi_2O_3–ZnO–Nb_2O_5) composition was mainly composed of orthorhombic

Table 1
Phase evolution of xBi_2O_3–ZnO–Nb_2O_5 compositions annealed at various temperatures for 1 h

Composition x		500 °C	600 °C	700 °C	750 °C	800 °C	900 °C
2	A1	BN1	BN1	BN1	BN1	BN2	BN2
				BN2	BN2	O–BZN	O–BZN
					BN3		
1.5	A2	BN1	BN1	BN1	BN1	BN2	O–BZN
			BN2	BN2	BN2	BN3	
						O–BZN	
1.25	A3	BN1	BN1	BN1	BN2	BN2	O–BZN
			BN2	BN2	BN3	BN3	C–BZN
					C–BZN	C–BZN	
						O–BZN	
1	A4	BN1	BN1	BN1	BN2	BN3	C–BZN
			BN2	BN2	BN3	C–BZN	
					C–BZN		
0.78	A5	BN1	BN1	BN1	BN2	BN3	BN3
				BN2	BN3	C–BZN	C–BZN
				BN3	C–BZN		

BN1: $Bi_{1.7}Nb_{0.3}O_{3.3}$; BN2: $Bi_5Nb_3O_{1.5}$; BN3: $BiNbO_4$. O–BZN: orthohombic pyrochiore phase. C–BZN: cubic pyrochotre phase.

O–BZN and cubic C–BZN pyrochlores. With decreasing Bi_2O_3 content, the A4 (1 Bi_2O_3–ZnO–Nb_2O_5) composition tends to form C–BZN. As the Bi_2O_3 content is further reduced, the Bi_2O_3-deficient composition such as A5 (0.78Bi_2O_3–ZnO–Nb_2O_5) leads to the formation of a residual phase $ZnNb_2O_6$ phase as shown in Fig. 1.

The phase evolution of xBi_2O_3–ZnO–Nb_2O_5 compositions with annealing temperatures at 500–900 °C is summarized in Table 1. At 500 °C, the BN1 phase was always first formed irrespective of compositions according to the report of JCPD.[15] With raising temperature to 600°C, the BN2 phase was subsequently developed. However, the formation and the stability of BN2 phase are found dependent on the bismuth content. The BN2 phase is always observed along with the formation of O–BZN phase in the bismuth-rich BZN composition such as A1.

For A2 composition, the phase evolution with annealing temperatures was shown in Fig. 2. The XRD patterns indicate that the BN1 phase first develops at the lower temperature below 500 °C. With increasing annealing temperature, the BN1phase gradually disappears along with the formation of BN2 phase at 600 °C. At 750 °C,the BN3 phase starts to form. Above 800 °C, the O–BZN phase develops. This indicates that the formation of O–BZN phase was probably interrelated with the simultaneous existence of BN2 and BN3 phases.

As the Bi_2O_3 content was further reduced from $Bi_2(Zn_{1/3}Nb_{2/3})_2O_7$ composition, i.e., A3, it was observed that the phase evolution is more complex. Below 700 °C, both BN1 and BN2 phase could be detected in A3 composition. At 750 °C, C–BZN phase starts to form and BN3 phase is developed, indicating that C–BZN phase is possibly transformed from the mixture phases of BN1 and BN2. Subsequently, at 800 °C, the peaks for O–BZN phase are identified. It reveals that C–BZN phase is more easily developed at

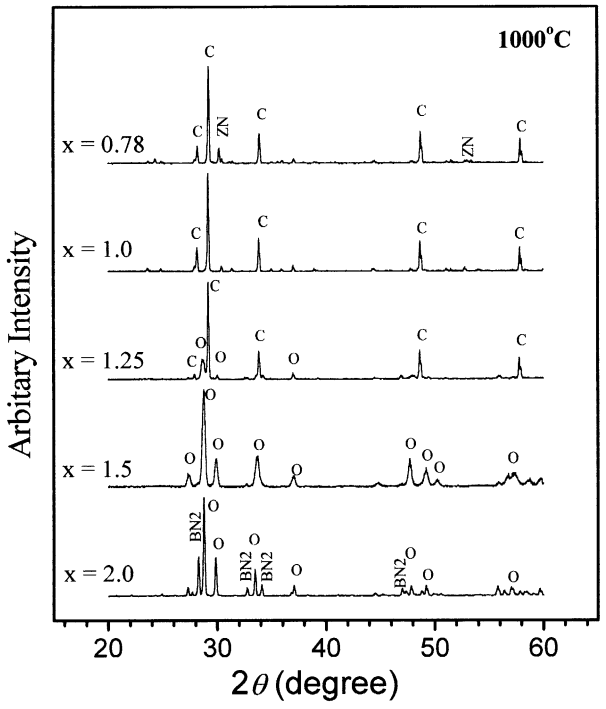

Fig. 1. XRD patterns for xBi_2O_3–ZnO–Nb_2O_5 system with $x = 0.78$–2.0 compositions annealed at 1000 °C for 1 h; BN2: $Bi_5Nb_3O_{15}$, BN3: $BiNbO_4$; ZN: $ZnNb_2O_6$, O: O–BZN, C: C–BZN.

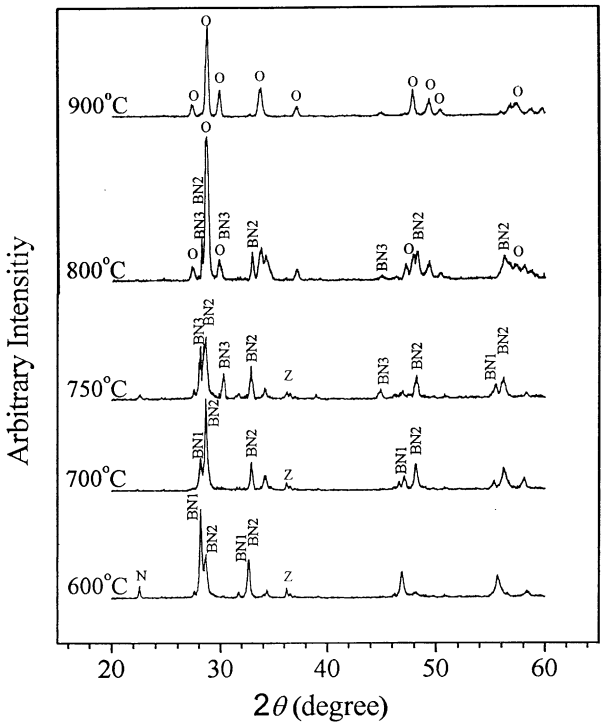

Fig. 2. XRD patterns for O–BZN phase evolution with annealing temperatures.

lower temperature than O–BZN phase. At 900 °C, even though both BN2 and BN3 phases disappear, both O– and C–BZN pyrochlore phases remain stable.

For the $(Bi_{1.5}Zn_{0.5})(Zn_{0.5}Nb_{1.5})O_7$ composition (A4), the XRD patterns in Fig. 3 show that at 500 °C, only BN1 intermediate phase was identified and followed by BN2 phase formation at 600 °C. As the A4 composition was annealed at ~750 °C, C–BZN phase starts to form. At 800 °C, in contrast to A3 composition, no O–BZN phase was detectable but only C–BZN phase with smaller BN3 amount was produced. However, we also found that the BN3 phase can be further reduced with increasing sintering temperature. As the Bi_2O_3 content was further decreased, although the A5 composition shows the same phase transitions as the A4composition, a single pure C–BZN phase cannot be formed even annealed at higher temperatures.

The Bi–Nb intermediate oxide phases (BN1, BN2 or BN3) depend on the bismuth content in Bi_2O_3–ZnO–Nb_2O_5 composition, which would influence the subsequent formation of pyrochlore phase type; O–BZN or C–BZN. The detailed formation mechanism and dominant intermediate phase for O–BZN or C–BZN phases would be discussed in the following.

3.2. Formation mechanism of C–BZN and O–BZN phases

In order to investigate the formation mechanisms for both $Bi_2(Zn_{1/3}Nb_{2/3})_2O_7$ (O–BZN) and $(Bi_{1.5}Zn_{0.5})(Zn_{0.5}Nb_{1.5})O_7$ (C–BZN) phases, the relative percentage of formed phases as a function of isothermal soaking time was determined based on the Eq. (1) as shown in Figs. 4 and 5. Fig. 4(a) and (b) shows the relationship between the formed percentage of individual phase and the soaking time at 750 °C and 800 °C for A4 composition, respectively. Fig. 4(a) illustrates that, at 750 °C, only both BN1 and BN2 phases can be detected in a very short time, i.e., 2 min. With increasing soak time, the BN1 phase gradually disappears but the amount of the BN2 increases up to a maximum at around 25 min, at which C–BZN phase starts to develop but BN2 phase presents a rapid decrease. We also observe that BN3 phase initiates at about 10 min and then increases with increasing soaking time. This observation might suggest that the BN2 phase has played an important role in the early reaction stage of C–BZN phase formation.

As the annealing temperature increases up to 800 °C, as shown in Fig. 4(b), it was found that not only BN1 and BN2 phases but also BN3 phase have already formed in a very short time, i.e. 2 min. However, after soaked more than 10 min, a rapid decrease of BN2 phase is accompanied by the continuous formation of both BN3 and C–BZN phases, indicating that the latter two phases are probably evolved from the former phase. Apparently, in the early stage, the formation of C–BZN is major due to direct evolution from BN2 phase. However, it was noted that after 15 min, although the BN2 phase nearly disappears, the detected amount of

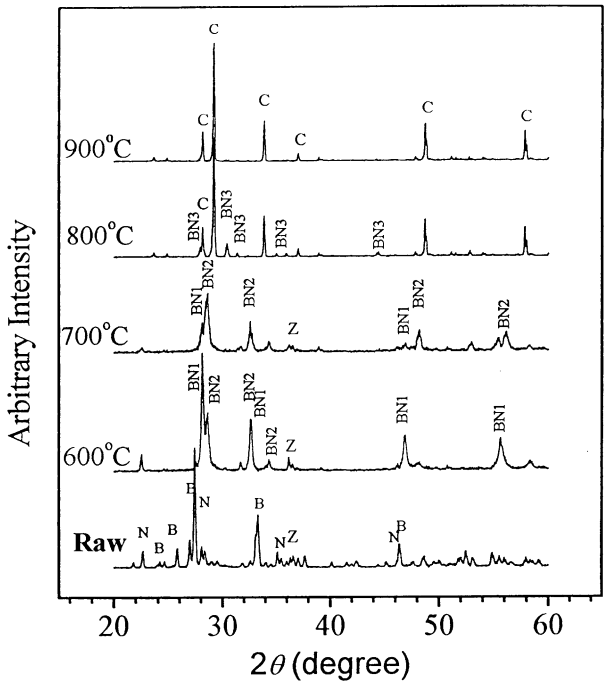

Fig. 3. XRD patterns for C–BZN phase evolution with annealing temperatures. (N: Nb_2O_5; B: Bi_2O_3, Z: ZnO).

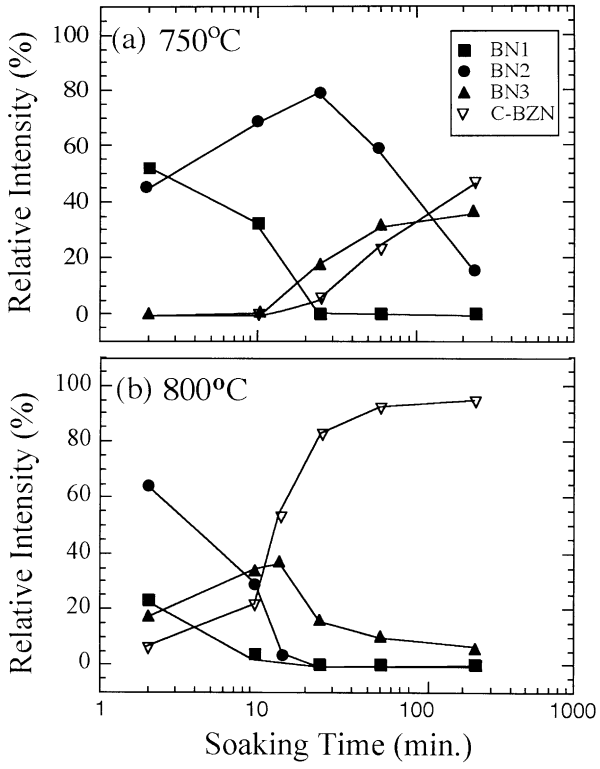

Fig. 4. Relationship between soaking time and intermediate phase content for A4 composition annealed at (a) 750 °C and (b) 800 °C.

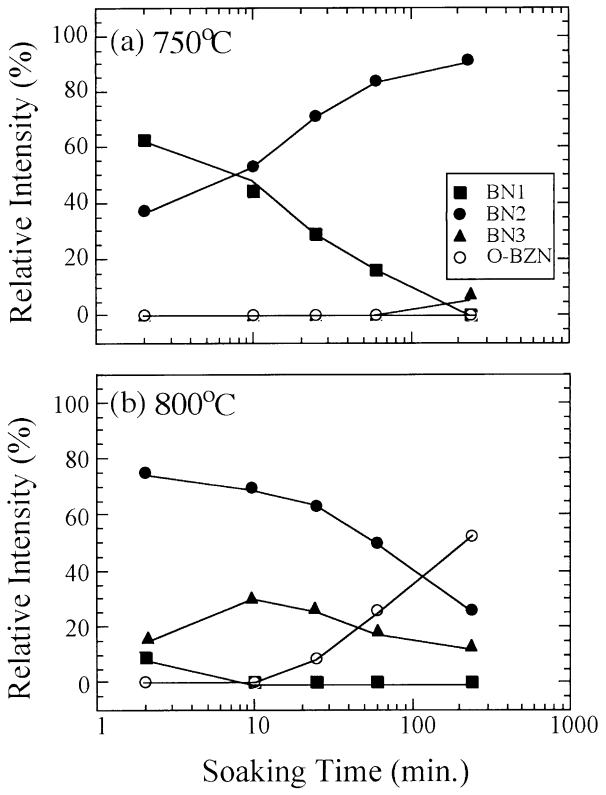

Fig. 5. Relationship between soaking time and intermediate phase content for A2 composition annealed at (a) 750 °C and (b) 800 °C.

C–BZN phase presents a continuous increasing but the BN3 phase rapidly decreases. The phenomenon reveals that the phase formation of C–BZN could be possibly contributed from BN3 phase. Interestingly, it was found that the transition occurs at 50∼65% C–BZN phase content. These results indicate that both BN2 and BN3 phases play equally important roles in C–BZN phase formation. Obviously, the formation of C–BZN phase is dominated by BN2 and BN3 phase at the earlier and later stages, respectively.

On the other hand, the phase evolution of A2 composition shown in Fig. 5(a) indicates that the phase formation of BN2 is always accompanied by the reduction of BN1 phase at 750 °C. Even soaked at a longer time, i.e., 240 min, only the BN2 phase is detected. Obviously, the annealing temperature of 750 °C is not high enough for promoting the formation of O–BZN phase. At 800 °C [Fig. 5(b)], both BN2 and BN3 phases can be detected in a very short time. The former phase gradually diminished with soaking time but the latter phase reversed. Prior to 10 min, the XRD pattern shows no O–BZN phase, indicating that an incubation time was apparently required for O–BZN phase formation. After 25 min, a rapid increase of O–BZN phase is observed and accompanied with the rapid decrease of BN2 and BN3 phases. These observations might reveal that there exists a close relationship between BN2/BN3 and O–BZN phases. It can be concluded that both BN2 and BN3 phase instead of either BN2 or BN3 phases as in the case of C–BZN mainly dominate the formation of O–BZN phase.

Even though the chemical reactions for the formation of both C–BZN and O–BZN phases have been reported by Wang et al.[12] both detailed reaction mechanisms and the role of Bi-Nb oxides in the pyrochlore formation of C–BZN and O–BZN phases have not been thoroughly studied. According to our results in Table 1, it shows that the type of pyrochlore phase formation, i.e., O–BZN or C–BZN, is strongly dependent on Bi_2O_3 content in the Bi_2O_3–ZnO–Nb_2O_5 system and the reaction mechanisms should be different for these pyrochlore phases. Additionally, Figs. 4 and 5 reveal that the intermediate Bi–Nb–O oxides to dominate the type of pyrochlore phase are also different. As shown in Fig. 4(a), the C–BZN phase can be developed from the BN2 phase without the presence of BN3 phase. However, in the later stage of C–BZN phase formation, although the BN2 phase has exhausted out, the C–BZN phase can be still produced in the presence of BN3 phase. Therefore, it can be postulated that either BN2 or BN3 phases dominate the formation of C–BZN phase. On the other hand, for the phase formation of O–BZN, Fig. 5(a) illustrates that although the BN2 has been formed, no detectable O–BZN phase can be observed even annealing the powder sample at 750 °C for a longer time. However, at 800 °C, with the presence of both BN2 and BN3 phases, the O–BZN phase can be developed, indicating that both BN2 and BN3 are simultaneously required for O–BZN phase formation. Therefore, both phase formation mechanisms of $(Bi_{1.5}Zn_{0.5})(Zn_{0.5}Nb_{1.5})O_7$ (C–BZN) and $Bi_2(Zn_{1/3}Nb_{2/3})_2O_7$ (O–BZN) can be summarized as follows:

(a) $(Bi_{1.5}Zn_{0.5})(Zn_{0.5}Nb_{1.5})O_7$ (C–BZN) pyrochlore phase:

$$5Bi_2O_3 + Nb_2O_5 \rightarrow 6Bi_{1.7}Nb_{0.33}O_{3.3} \qquad 400\ ^\circ C < T < 600\ ^\circ$$
$$3Bi_{1.7}Nb_{0.33}O_{3.3} + Nb_2O_5 \rightarrow Bi_5Nb_3O_{15} \qquad 600\ ^\circ C < T < 750\ ^\circ C$$
$$Bi_5Nb_3O_{15} + Nb_2O_5 \rightarrow 5BiNbO_4 \qquad 750\ ^\circ C < T < 800\ ^\circ C$$
$$Bi_5Nb_3O_{15} + 2ZnO \rightarrow 2Cub.(Bi_{1.5}Zn_{0.5})(Zn_{0.5}Nb_{1.5})O_7 + Bi_2O_3 \qquad 750\ ^\circ C < T < 800\ ^\circ C$$

or

$$\tfrac{3}{2}BiNbO_4 + ZnO \rightarrow Cub.(Bi_{1.5}Zn_{0.5})(Zn_{0.5}Nb_{1.5})O_7 \qquad 800\ ^\circ C < T < 850\ ^\circ C$$

(b) $Bi_2(Zn_{1/3}Nb_{2/3})_2O_7$ (O–BZN) pyrochlore phase:

$$5Bi_2O_3 + Nb_2O_5 \rightarrow 6Bi_{1.7}Nb_{0.33}O_{3.3} \qquad 400\ ^\circ C < T < 600\ ^\circ C$$
$$3Bi_{1.7}Nb_{0.33}O_{3.3} + Nb_2O_5 \rightarrow Bi_5Nb_3O_{15} \qquad 600\ ^\circ C < T < 750\ ^\circ C$$
$$Bi_5Nb_3O_{15} + Nb_2O_5 \rightarrow 5BiNbO_4 \qquad 750\ ^\circ C < T < 850\ ^\circ C$$
$$Bi_5Nb_3O_{15} + BiNbO_4 + 2ZnO \rightarrow 3Bi_2(Zn_{2/3}Nb_{4/3})O_7 \qquad 800\ ^\circ C < T < 900\ ^\circ C$$

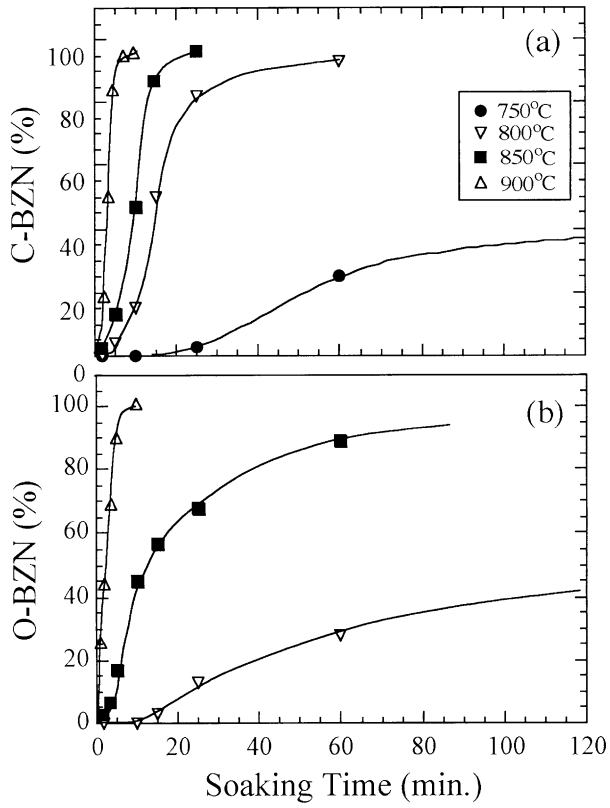

Fig. 6. Isothermal transformation kinetics of (a) A4 and (b) A2compositions annealed at various temperatures.

3.3. Reaction kinetics of C–BZN and O–BZN phaseformation

The relative percentage of formed $(Bi_{1.5}Zn_{0.5})(Zn_{0.5}Nb_{1.5})O_7$ (C–BZN) and $Bi_2(Zn_{1/3}Nb_{2/3})_2O_7$ (O–BZN) phases under isothermal heat treatment was calculated according to the Eq. (1). Fig. 6 shows that a sigmoid shape, which signifies the existence of an incubation time before a measurable phase, characterizes the solid-state reaction of pyrochlore phases. The results indicate that the reaction is a diffusion-controlled mechanism and minimum activation energy is required. It can be seen that the formed pyrochlore content increases with increasing temperature and soaking duration. From Fig. 6(a), as corresponding to aforementioned results, the C–BZN phase begins to develop at 750 °C after 25-min incubation. When the calcinaton temperature was raised to 800 °C, the required incubation is very short about 1∼2 min, and a complete formation of C–BZN phase required 50∼60 min. For a higher calcination temperature, i.e., 850 °C, it took only ∼25 min to obtain a maximum content of C–BZN phase. In the other case of O–BZN phase formation, as shown in Fig. 6(b), the starting temperature of O–BZN phase formation is about 800 °C, which is slight higher than that of C–BZN phase. An incubation time was still required to nucleate the O–BZN phase embryos. It was found that the formation rate of O–BZN phase, if based on the same annealing temperature, is slower than that of C–BZN phase. It took more than 100∼120 min. to reach a maximum content at 850 °C. These results indicate that reaction kinetics between C–BZN phase and O–BZN phase formation should be different.

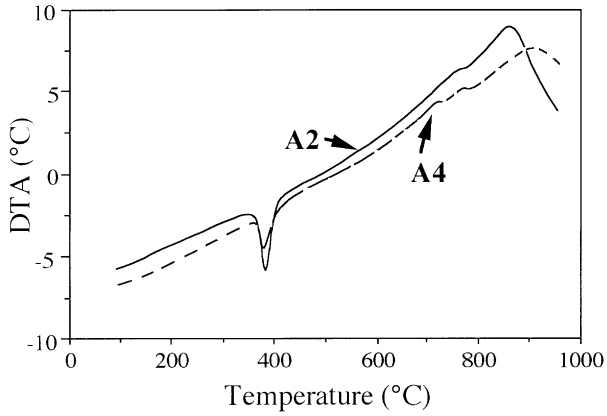

Fig. 7. DTA curves of both A2 and A4compositions at a heating rate of 10 °C/min.

Referring to the DTA results of Fig. 7, it can be observed that the reaction for C–BZN phase is more complex than O–BZN phase. Two smaller exothermic reaction peaks around 700–800 °C were observed in the $(Bi_{1.5}Zn_{0.5})(Zn_{0.5}Nb_{1.5})O_7$ (A4) composition for C–BZN phase formation. Those peaks may be corresponding to the formation of BN3 and Zn-rich C–BZN phases as evidenced from Fig. 4(b). The formation of both BN3 and C–BZN phases was accompanied with the rapid decrease of BN2 due to its reaction with ZnO after a longer soaking time at 750 °C.

Since the used materials are multiphase, the formation reaction of either C–BZN or O–BZN phase belongs to heterogeneous system. A model used to treat multiphase reaction kinetics was derived by Johnson and Mehl[16] and by Avrami[17] as follows:

$$\ln[1/(1-y)] = (kt)^n$$

where y is the formation content of BZN pyrochlore phase, k the reaction rate constant, t the reaction time and n the reaction order. This model has been widely and successfully used in multiphase systems for analysis of reaction kinetics.[18,19] Further calculation from the data shown in Fig. 6 can be replotted as ln{ln[1/(1−y)]} vs. ln (t) for both C–BZN and O–BZN phase systems, as shown in Fig. 8(a) and (b), respectively. Noted that as the samples were annealed at a lower temperature below 800 °C, two straight segments can be observed because of slower reaction kinetics, which can be treated as a two-stage process in the formation of BZN pyrochlore phase. Since the reaction in stage 2 plays a less impor-

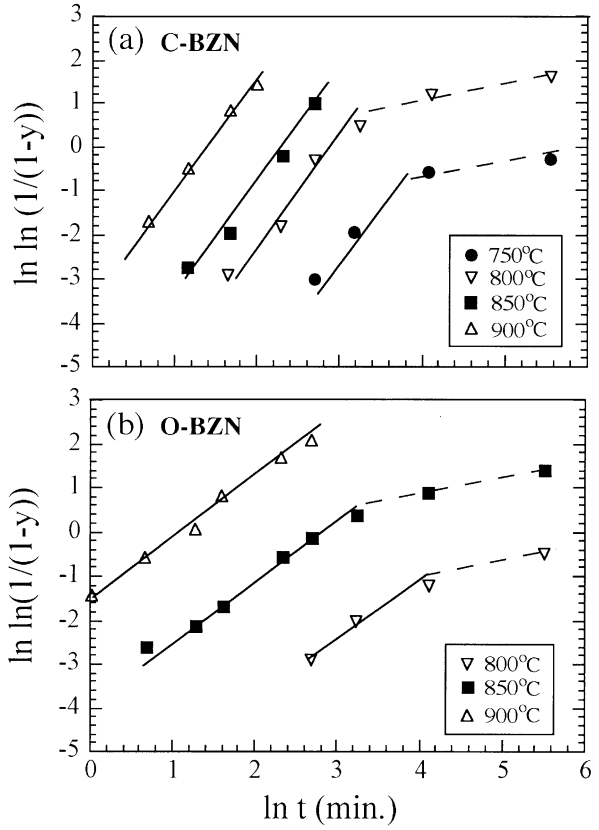

Fig. 8. Johnson–Mehl–Avrami plots of the kinetic data for (a) C–BZN and (b) O–BZN phase formation.

tant role, the reaction kinetics occurring in stage 1 will be focused. In this stage, the reaction orders (n values) are 2.47 and 1.65 for C–BZN and O–BZN phase formation, respectively. This indicates that the reaction mechanisms and the controlling factors are different.

According to Johnson–Mehl–Avrami model, the n value around 2.5 for the reaction of C–BZN phase presents diffusion controlled growth with constant nucleation rate.[17,20–22] From Fig. 4, it can be observed that the C–BZN phase formation is not only going through BN2 transition, but also the BN3 phase also makes contributions on the C–BZN phase formation. Furthermore, as mentioned above, BN3 phase formation possibly results from the transformation of BN2 phase. This fact again demonstrates that BN2 and BN3 phases play an important role in C–BZN phase formation during the calcination. Therefore, a heterogeneous nucleation was promoted since more than these two phases exist in the $(Bi_{1.5}Zn_{0.5})(Zn_{0.5}Nb_{1.5})O_7$ composition. Consequently, the formation reaction in the C–BZN phase can be considered as diffusion controlled process with constant nucleation rate.

On the other hand, the n value of $\sim$1.5 reveals that the reaction of O–BZN phase is possibly diffusion controlled process with zero nucleation rate. This formation behavior of O–BZN phase can be reasonably explained with the Fig. 5(a) as one can see. Without the BN3 phase, although BN2 phase has been formed, the O–BZN phase can not be produced. In other words, the O–BZN phase formation can be interpreted as due to the simultaneous contribution from the reaction of BN2 and BN3 phases. Therefore, the provided nuclei for O–BZN phase are limited prior to the formation of O–BZN. Consequently, the reaction formation of O–BZN phase could be thought as diffusion controlled process with zero nucleation rates.

The temperature dependence of reaction rate constant k can be represented by the Arrhenius equation, i.e., $k \propto \exp(-Q/RT)$, where the activation energy (Q) can be obtained from the curve of $ln\ k$ vs. 1/T. The activation energy ($Q = \sim 450$ kJ/mol) of C–BZN phase is smaller than that ($Q = \sim 602$ kJ/mol) of O–BZN phase. This could be confirmed by firing the A2 composition at higher temperature more than 1100 °C. The composition should be corresponding to the formation of O–BZN phase as annealed at 800–850 °C. However, it was found that a mixture of O–BZN and C–BZN phases was detected instead of single O–BZN phase. Once the cubic pyrochlore forms, the transformation of the cubic phase (C–BZN) to pseudo-tetragonal phase (O–BZN) cannot be triggered by heating at lower temperature. The phenomenon suggests that higher activation energy is possible related to crystal structure. Since A sites in the $A_2B_2O_7$ as in $Bi_2(Zn_{1/3}Nb_{2/3})_2O_7$ pyrochlore structure are occupied by Bi^{3+} ions only, the $6s^2$ lone pair electrons would lead to the distortion of the cell. Therefore, larger activation energy was required for the formation of distorted orthorhombic (O–BZN) phase as compared to cubic C–BZN phase.

3.4. Characteristics and microwave properties

As mentioned before, in Bi_2O_3–ZnO–Nb_2O_5 (BZN) system, it was reported that bismuth content exhibits a great effect on the pyrochlore phase formed. Therefore, the effect of bismuth content on characteristics and microwave properties of BZN ceramics will be further studied to elucidate the role of crystal structure. For comparison, BZN ceramics were sintered at 1000 °C for 1 h. Based on the crystal structure and lattice parameters of BZN phase, the calculated densities were 7.11g and 7.94 g/cm^3 for C–BZN and O–BZN phases, respectively.[12] Fig. 9 shows that the bulk density of 6.79 g/cm^3 for A4 ($x = 1$ in the xBi_2O_3–ZnO–Nb_2O_5 system) composition with single C–BZN phase corresponds to the theoretical density of 95.5%. Similarly, under the same sintering condition, A2 ($x = 1.5$) composition with single O–BZN phase gives a bulk density of 7.71 that is about 97.1% theoretical density. The C–BZN or O–BZN phase content in Fig. 9 was calculated based on Eq. (1). The reduction of C–BZN phase content in A5 composition ($x = 0.78$) as com-

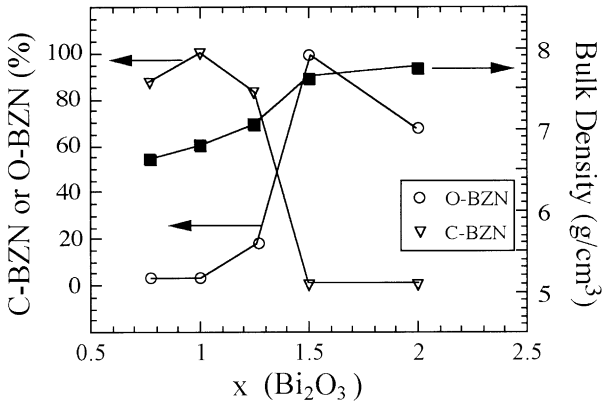

Fig. 9. Effect of $x(Bi_2O_3)$ content on phase content and bulk density of xBi_2O_3–ZnO–Nb_2O_5 ceramics sintered at 1000 °C for 1 h.

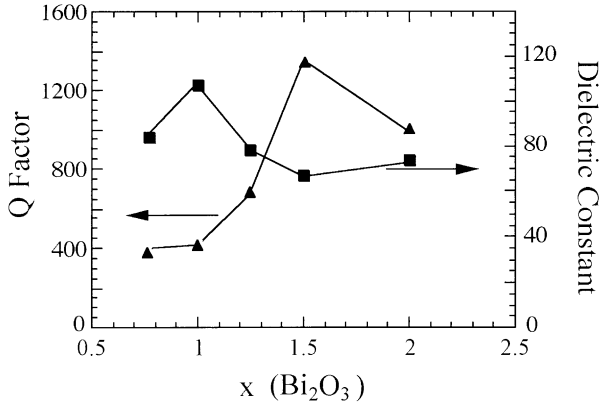

Fig. 10. Effect of $x(Bi_2O_3)$ content on microwave properties of xBi_2O_3–ZnO–Nb_2O_5 ceramics sintered at 1000 °C for 1 h.

pared to A4 composition ($x=1$) is probably due to $ZnNb_2O_6$ phase formation as evidenced from Fig. 1. Similarly, for the BZN composition with $x=2$ (A1), the decreased amount of O–BZN phase is partially attributed to the forming of BZN-containing Bi_2O_3 phase, which is very close to BN2 phase. However, the increase in bulk density was obviously related to BZN Bi_2O_3-containing BZN phase since Bi_2O_3 like PbO is well known to have a lower melting point, which in turn enhances sintering densification, and therefore, a higher density was easily obtained in the bismuth-rich composition. Therefore, as the Bi_2O_3 content increased from $x=1.0$ to 1.5, the formed O–BZN phase content makes a jump increase and the bulk density was also enhanced.

Fig. 10 illustrates that C–BZN phase always exhibits a higher dielectric constant than O–BZN phase. This might be related to O–BZN crystal structure, as mentioned previously, O–BZN phase belongs to a distorted orthorhombic structure. The smaller dielectric constant in O–BZN phase may be attributed to the more distorted nature, which generally suppresses the polarizability of ions with increasing the distortion. Therefore, a sharp decrease in dielectric constant corresponding to the phase transition from C–BZN to O–BZN phase is observed. The decrease of dielectric constant in A5 than A4 can be reasonably explained with the formation of $ZnNb_2O_6$ phase, in which the dielectric constant is about 25 and much smaller than C–BZN phase.[23] On the other hand, as compared with A2 composition, the slight increase in dielectric constant in A1 composition can be attributed to its higher bulk density. From Fig. 10, it can be observed that Q values were strongly interrelated with phase structure existed in the compositions. The O–BZN phase gives a larger Q values than C–BZN phase. However, as the composition contains a second phase, the Q value was much reduced. Therefore, even though A1 composition ($x=2$) has a higher bulk density, the Q value becomes smaller than that of A2 ($x=1.5$) composition due to the existence of Bi_2O_3-containing Bi_2O_3 BZN phase.

4. Conclusions

Some conclusions were drawn from the study of phase transformation and reaction kinetics in the Bi_2O_3–ZnO–Nb_2O_5 (BZN) system especially on both $Bi_2(Zn_{1/3}Nb_{2/3})_2O_7$ (O–BZN) and $(Bi_{1.5}Zn_{0.5})(Zn_{0.5}Nb_{1.5})O_7$ (C–BZN) phases.

(1) The Bi_2O_3 content plays a very important role in crystal structure and phase transformation of BZN ceramics.
(2) Kinetics studies indicate that both BN2 and BN3 phases are simultaneously required for the formation of O–BZNphase but the formation of C–BZN phase can be developed from either BN2 or BN3 phases.
(3) The formation of O–BZN phase belongs to diffusion controlled reaction with a zero nucleation rate. On the other hand, C–BZN phase should be diffusion controlled reaction with a constant nucleation rate.
(4) C–BZN phase has a lower activation energy and formation temperature than O–BZNphase.
(5) C–BZN phase exhibits a higher dielectric constant but a lower Q value as compared with O–BZNphase.

Acknowledgements

The authors would like to thank the financial support from the National Science Council of the Republic of China under Contract No. NSC89–2213-E-009–080.

References

1. Matsumoto, K., Hiuga, T., Takada, K. and Ichimura, H. Proc. 6th IEEE. International Symposium on Application of Ferroelectrics, 1986, 118.
2. Plourde, J. K., Linn, D. F., O'Bryan, H. M. Jr. and Thomson, J., *J. Am. Ceram. Soc*., 1975, **58**, 418.
3. Kagata, H., Inoue, T., Kato, J. and Kameyama, I., *Jpn. J. Appl. Phys*, 1992, **31**, 3152.
4. Wang, Z. and Zhang, S. *Proceedings of the 37th Electronic Components Conference*; Catalog No. 87CH2448–9, 1987, 413.
5. Hagemann, H. J., Hennings, D. and Wernicke, R., Ceramic multilayer capacitors. *Philips Tech. Rev*., 1984, **41**, 89.
6. Ling, H. C., Yan, M. F. and Rhoeds, W. W., *J. Mater, Res*., 1990, **5**, 1752.
7. Yan, M. F., Ling, H. C. and Rhodes, W. W., *J. Am. Ceram. Soc*., 1990, **73**, 1106.
8. Liu, D., Liu, Y., Huang, S.-Q. and Yao, X., *J. Am. Ceram. Soc*., 1993, **76**, 2129.
9. Swartz, S.L. and Shrout, T.R. US Patent 5449652, 1995.
10. Subramanian, M. A., Aravamudan, G. and Subba Rao, G. V., Oxide pyrochlore—a review. *Prog. Solid State Chem*., 1983, **15**, 55.
11. Wang, H., Wang, X. and Yao, X., Cubic pyrochlore structure in the Bi_2O_3–ZnO–Nb_2O_5-system. *J. Chin. Ceram. Soc*., 1995, **23**, 241.
12. Wang, X., Wang, H. and Yao, X., *J. Am. Ceram. Soc*., 1997, **80**, 2745.
13. Hakki, B. W. and Coleman, P. D., *IRE Trans. Microwave Theory Technol., MTT*-, 1960, **8**, 402.
14. Courtney, W. E.. *IEEE Trans. Microwave Theory Technol., MTT18, 1970, 476–485*.
15. ASTM JCPDS File No. 33–0210, 1997.
16. Johnson, W. A. and Meh, R. F., *Trans. AIME*, 1939, **135**, 416.
17. Avrami, M., *J. Chem. Phys*, 1939, **7**, 1103.
18. Jean, J.-H. and Lin, S.-C., *J. Mater. Res*., 1999, **14**, 2922.
19. Ohshima, N., *J. Appl. Phys*, 1996, **79**, 8357.
20. Avrami, M., *J. Chem. Phys*, 1940, **8**, 212.
21. Avrami, M., *J. Chem. Phys*, 1941, **9**, 177.
22. Christian, J.W. *The Theory of Transformations in Metals and Alloys*. Pergamon, London, 1965, pp. 525–548.
23. Lee, H.-J. and Hong, K.-S., *J. Mater. Res*., 1997, **12**, 1437.